Article

Probing Capacity Trends in MLi$_2$Ti$_6$O$_{14}$ Lithium-Ion Battery Anodes Using Calorimetric Studies

K. Jayanthi, Anshuman Chaupatnaik, Prabeer Barpanda, and Alexandra Navrotsky*

Read Online

ACCESS | Metrics & More | Article Recommendations | SI Supporting Information

ABSTRACT: Due to higher packing density, lower working potential, and area specific impedance, the MLi$_2$Ti$_6$O$_{14}$ (M = 2Na, Sr, Ba, and Pb) titanate family is a potential alternative to zero-strain Li$_4$Ti$_5$O$_{12}$ anodes used commercially in Li-ion batteries. However, the exact lithiation mechanism in these compounds remains unclear. Despite its structural similarity, MLi$_2$Ti$_6$O$_{14}$ behaves differently depending on charge and size of the metal ion, hosting 1.3, 2.7, 2.9, and 4.4 Li per formula unit, giving charge capacity values from 60 to 160 mAh/g in contrast to the theoretical capacity trend. However, high-temperature oxide melt solution calorimetry measurements confirm strong correlation between thermodynamic stability and the observed capacity. The main factors controlling energetics are strong acid−base interactions between basic oxides MO, Li$_2$O and acidic TiO$_2$, size of the cation, and compressive strain. Accordingly, the energetic stability diminishes in the order Na$_2$Li$_2$Ti$_6$O$_{14}$ > BaLi$_2$Ti$_6$O$_{14}$ > SrLi$_2$Ti$_6$O$_{14}$ > PbLi$_2$Ti$_6$O$_{14}$. This sequence is similar to that in many other oxide systems. This work exhibits that thermodynamic systematics can serve as guidelines for the choice of composition for building better batteries.
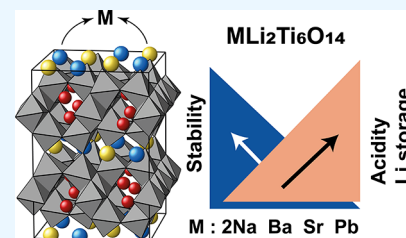
INTRODUCTION

Lithium-ion batteries (LIBs) are the currently favored power sources for portable applications such as electric vehicles and electronic products.[1] Most commercial LIBs work via reversible intercalation[2] of lithium ions between a (mixed) transition metal oxide cathode and a layered graphite anode.[3] For more than 30 years since the inception of LIBs by SONY (Tokyo, Japan) in the 1990s, graphite remains the most widely used and optimized anode material due to its high theoretical capacity (380 mAh/g) and low Li insertion voltage (ca. 0.2 V) while maintaining an intercalation mechanism, which guarantees structural integrity and long cycle life. Nevertheless, the graphite anode has several issues, such as solvent-dependent stability,[4,5] large volume change, large irreversible capacity loss (ICL) from solid electrolyte interphase (SEI) formation (below 0.8 V),[6] and fire risk due to lithium plating during overcharge or higher currents[7] some of which directly stem from its low voltage performance.

In this context, the zero-strain spinel Li$_4$Ti$_5$O$_{12}$ anode operating at flat and higher voltage (1.55 V vs Li, 175 mAh/g) was introduced[8,9] and is commercially preferred[10] over graphite in applications requiring fast charging and safety. Additionally, Li$_5$Cr$_7$Ti$_6$O$_{25}$ similar to Li$_4$Ti$_{15}$O$_{12}$ spinel synthesized at 800 °C exhibits large charge capacity, good cycle stability, superior rate performance, and outstanding electrochemical kinetics. When cycled at 200 mA/g, it displays a high initial reversible capacity of 146.6 mAh/g and retains a considerable capacity of 130.8 mAh/g after 300 cycles.[11] Among other Ti-based electrode materials,[12−14] MLi$_2$Ti$_6$O$_{14}$ (M = 2Na, Sr, Ba, and Pb)[15−17] shows lower voltage (1.28−1.42 V vs Li), low area specific impedance,[16] and higher

packing density[18] than Li$_4$Ti$_5$O$_{12}$ and has a high theoretical capacity (220−282 mAh/g) for redox activity of all six Ti (Figure 1i).[19] The MLi$_2$Ti$_6$O$_{14}$ series exhibit open channels enabling reversible Li$^+$ insertion in vacant sites like 8c, 4a, and 4b of the orthorhombic framework (Cmca). However, the observed capacity trend in this series does not follow the theoretical capacity trend. Previous studies identified crystallographic origins underlying the low capacity of the monovalent member (M = 2Na) vs the divalent members (M = Ba, Sr, and Pb).[16,17] However, currently there is no explanation of the anomalous trend of the observed capacity in the isostructural divalent members—BaLi$_2$Ti$_6$O$_{14}$ (2.7 Li) < SrLi$_2$Ti$_6$O$_{14}$ (2.9 Li) < PbLi$_2$Ti$_6$O$_{14}$ (4.4 Li)—where PbLi$_2$Ti$_6$O$_{14}$ is opposite to the theoretical capacity trend.

We take a new approach to understand the electrochemical property trend in this isostructural MLi$_2$Ti$_6$O$_{14}$ series from their relative thermodynamic stabilities, attempting to elucidate the structure−property relationships in this family of materials. High-temperature oxide melt solution calorimetry is an established methodology to measure the thermodynamic stabilities of oxide and nonoxide systems.[20−22] Recently, Abramchuk et al.[23] used this method to investigate the thermodynamic stability and its role in the mechanism of ionic
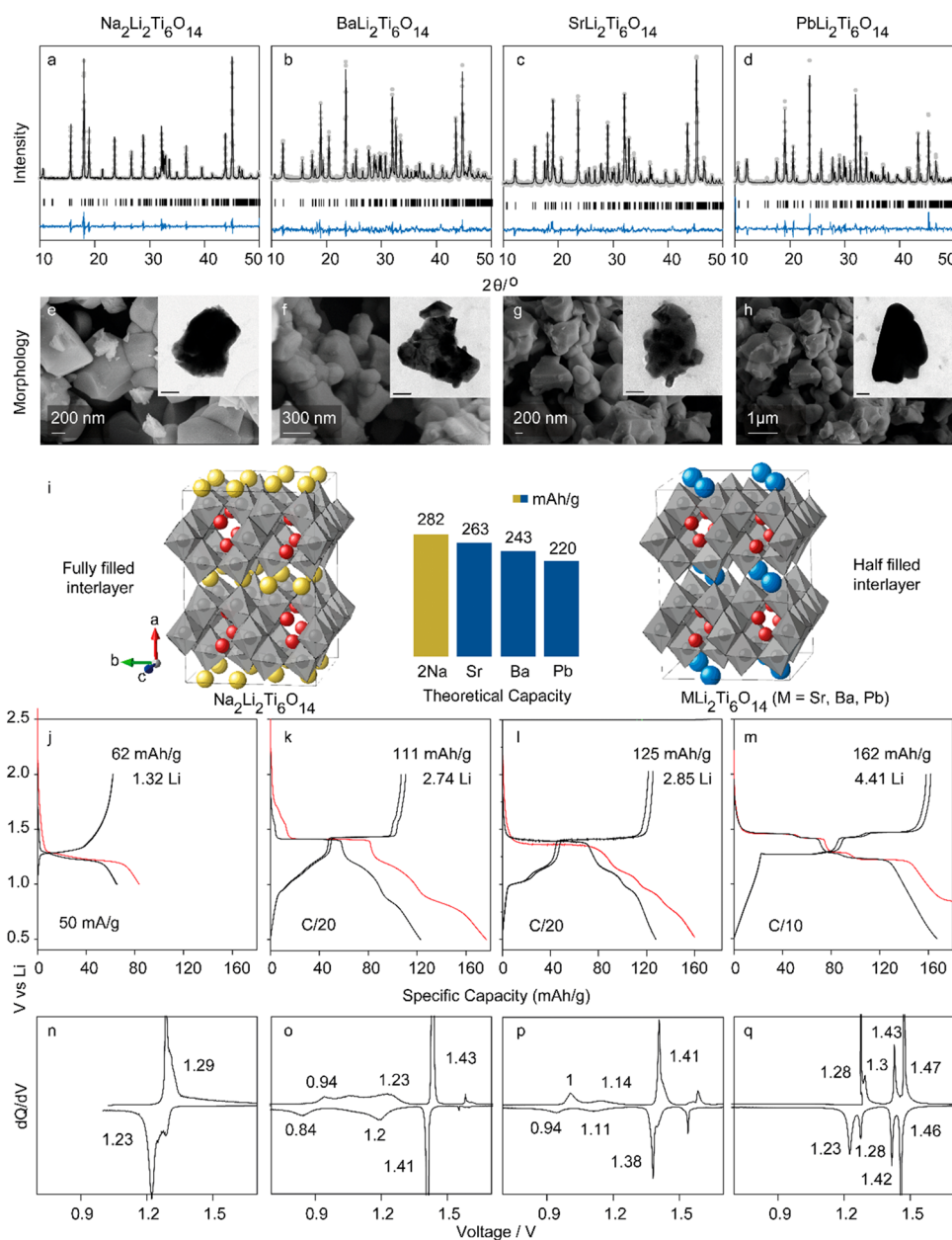
Figure 1. (a−d) Rietveld refinement of XRD (Cu Kα) patterns of members of the $MLi_2Ti_6O_{14}$ family (M = 2Na, Sr, Ba, and Pb) formed by solution combustion (900 °C, 2 h). Experimental data points (gray dots), calculated pattern (black), their difference (blue), and Bragg reflections (black bars) of the respective isostructural phases are shown. (e−h) SEM micrographs of the combustion synthesized $MLi_2Ti_6O_{14}$ anode indicating porous structure of secondary agglomerates. The inset shows a TEM image of primary nanometric particles (200 nm scale). (i) Structural illustration of the $MLi_2Ti_6O_{14}$ anodes. (j−m) Galvanostatic (dis)charge voltage profiles and (n−q) differential capacity plots depicting the electrochemical performance of the $MLi_2Ti_6O_{14}$ anodes.

transport in the NASICON-type solid-state electrolyte $Li_{1+x}Al_xTi_{2−x}(PO_4)_3$. They demonstrated a strong correlation between the energetic stability and ionic conductivity in LATPs with a pronounced change in the trends with composition. In the present work, we employ high-temperature oxide melt solution calorimetry to systematically assess the thermodynamic stability of $MLi_2Ti_6O_{14}$ (M = 2Na, Sr, Ba, and Pb), which provides insights into observed differences in the capacity. We found a strong correlation between the thermodynamic stability and reversible lithium insertion in $MLi_2Ti_6O_{14}$ anode materials and explain the trend in observed capacity. This work reflects the acid−base energetic contributions in this class of anode materials.

■ EXPERIMENTAL SECTION

Synthesis and Electrochemistry. $MLi_2Ti_6O_{14}$ was synthesized by a two-step solution combustion method. Metal nitrates as oxidizers (O) and glycine as fuel (F) were taken in a 1:1 ratio to ensure maximum exothermicity. Lithium nitrate ($LiNO_3$, Sigma-Aldrich, 99%), sodium nitrate ($NaNO_3$, SD Fine, 99.5%), barium nitrate ($Ba(NO_3)_2$, Sigma-Aldrich, >99%), lead nitrate ($Pb(NO_3)_2$, SD Fine, 99.5%), and strontium nitrate ($Sr(NO_3)_2$, Sigma-Aldrich, 99%) were used. Titanium (Ti^{4+}) ions were sourced from freshly prepared titanyl nitrate ($TiO(NO_3)_2$ as it is unstable).[24] This was made by simultaneous hydrolysis—nitration of titanium isopropoxide ($C_{12}H_{28}O_4Ti$, Sigma-Aldrich, 97%) in isopropyl alcohol

(Merck, analytical grade 99.7%) under ice-cold conditions. The mixture was heated to less than 150 °C to remove water and form a thick solution, which was reheated at 500 °C to trigger combustion. The resulting white intermediate powder was ground, pelletized, and annealed in air at 900 °C for 1 min to 2 h. The phase purity of combustion prepared $MLi_2Ti_6O_{14}$ samples was verified from powder X-ray diffraction patterns (2θ range = 10−50°, step size = 0.026° s^{-1}) obtained using a PANalytical X'Pert Pro X-ray diffractometer having a Cu-Kα source (λ_1 = 1.54 Å). Rietveld refinement was done using the GSAS program.[25] The structures were illustrated using the VESTA software.[26]

The surface morphology of the powders was characterized using a scanning electron microscope having a LaB$_6$ field emission source (Carl Zeiss ULTRA55 FESEM, 5 kV) and using a transmission electron microscope (FEI Tecnai F20 STwin, 200 kV). TG-DSC measurements were performed using a Setaram LABSYS EVO instrument. 25 mg of the powdered sample was pressed into a pellet, placed in a Pt crucible, and heated from 30 to 800 °C (10 °C/min) under a N$_2$ flow (20 mL/min). A buoyancy correction was performed with an empty crucible prior to the experiment. The pristine powder was ground with carbon (Super P, Sigma-Aldrich, 99+ %) and a polyvinylidene fluoride (PVDF) binder in an 80:10:10 or 70:20:10 weight ratio. This electrode powder was mixed with N-methyl-2-pyrrolidone (Sigma-Aldrich, >99%) solvent and drop cast onto prewashed Cu coupons. The electrodes were dried at 80 °C overnight in a vacuum oven and were used for assembling CR2032 coin cells vs lithium (Sigma-Aldrich, >99%) in an Ar-filled glovebox (MBraun LABStar GmbH). Whatman GF/C glass fiber was used as the separator and 1 M LiPF$_6$ in 1:1:3 v/v % of ethylene carbonate/propylene carbonate/dimethyl carbonate (EC/PC/DMC) (chameleon reagent) was used as the electrolyte. The cells were cycled between 2 V to 1 or 0.5 V at C/20 and 50 mA/g current using a Neware BTS-4000 battery cycler to ensure we reach the maximum specific capacity values for each of the materials, which can then be rationalized with the thermodynamic trend.

High-Temperature Oxide Melt Solution Calorimetry. High-temperature oxide melt solution calorimetry was performed using a Setaram AlexSYS Tian-Calvet twin microcalorimeter using methods standard to our laboratory and described previously.[20−22] This calorimeter allows the direct determination of the enthalpy of formation ($\Delta H^\circ_{f,ox}$) of multicomponent compounds from their binary oxides. In a typical experiment, ~5 mg of the $MLi_2Ti_6O_{14}$ sample was pelletized and dropped from ambient temperature into a calorimeter at 800 °C containing the solvent molten sodium molybdate ($3Na_2O\cdot4MoO_3$) in a platinum crucible. The measured enthalpy of drop solution (ΔH_{ds}) is the sum of the sample heat content from ambient temperature to 800 °C and its heat of solution in the solvent at 800 °C. At least 8−10 experiments were done per sample, and the results are reported as average values with error being two standard deviations of the mean. The calorimetry glassware was flushed with oxygen gas at a flow rate of 65 mL/min to maintain a constant atmosphere, and the solvent was bubbled with the same gas at 5 mL/min to remove liberated evolved gases, aid dissolution, and prevent local saturation of the solvent. The calorimeter was calibrated using the heat content of 5 mg of pellets of α-Al$_2$O$_3$ (99.997%). The details of the calorimeter and procedures have been described previously.[20−22]

RESULTS AND DISCUSSION

Structure and Electrochemical Performance. The combustion synthesized $MLi_2Ti_6O_{14}$ powders were found to be phase pure from Rietveld refinement (Figure 1a−d and Tables S1−S4, Supporting Information). The powders were well crystallized into primary particles of about 1 micron, which agglomerated to a porous network (Figure 1e,f). The crystal structure is orthorhombic (symmetry: Cmca), containing a three-dimensional network of TiO$_6$ octahedral units. Two edge-shared units along the b-axis stitch the infinite c-axis directed edge-shared units in a ladderlike way. The ladders form a sheet in the bc plane. In the sheet, inside each c-directed ladder, there is an empty tunnel where structural lithium ions sit in tetrahedral sites with adjacent octahedral sites free. This sheet is three units thick along the a-axis and is glued to other sheets via larger M ions which populate the interlayer partially (M = Sr, Ba, and Pb) or completely (M = 2Na). One unit of $MLi_2Ti_6O_{14}$ can host up to six lithium atoms, for complete reduction of Ti^{4+} to Ti^{3+}, offering a theoretical capacity of about 240 mAh/g depending on the atomic weight of M (Table 1). The mechanism of lithium insertion is unclear, and only about 75% of theoretical capacity has been attained.

Table 1. Space Group, Charge Capacity, and Li Uptake per Formula Unit of the $MLi_2Ti_6O_{14}$ Titanates

anode material	space group	charge capacity (mAh/g)	operating voltage (V) vs Li	Li uptake (per f.u.)
Na$_2$Li$_2$Ti$_6$O$_{14}$	Cmca	62	1.28	1.32
SrLi$_2$Ti$_6$O$_{14}$	Cmca	111	1.42	2.74
BaLi$_2$Ti$_6$O$_{14}$	Cmca	125	1.38	2.85
PbLi$_2$Ti$_6$O$_{14}$	Cmca	162	1.35	4.40

Na$_2$Li$_2$Ti$_6$O$_{14}$ is the lightest among $MLi_2Ti_6O_{14}$ (M = 2Na, Sr, Ba, and Pb) and so it is expected to have the highest theoretical capacity of 282 mAh/g for six Ti redox (Figure 1i). However, due to the geometrical constraints, it cannot insert more than two Li (62 mAh/g, 1.3 Li) as the vacant 11 coordinated interlayer sites are fully filled with two monovalent Na atoms, compared to the half-filled interlayer by one divalent M atom (M = Ba, Sr, and Pb) in the remaining members (enabling them to incorporate up to 4.4 Li) (Figure 1j−m). Furthermore, even the divalent counterparts with half-filled interlayers are space limited as they reversibly allow only four lithium ions (instead of six) via reduction of four out of six Ti ions. Lithium ions (de)insert from 1.2 to 1.5 V in the system, with each member showing its signature (de)insertion voltage (Figure 1n−q). The observed charge capacity is in the order BaLi$_2$Ti$_6$O$_{14}$ (111 mAh/g, 2.7 Li) < SrLi$_2$Ti$_6$O$_{14}$ (125 mAh/g, 2.9 Li) < PbLi$_2$Ti$_6$O$_{14}$ (162 mAh/g, 4.4 Li). While a slightly higher observable capacity in the Sr analog compared to Ba is in line with the trend in their theoretical capacity, the reason why PbLi$_2$Ti$_6$O$_{14}$ shows the largest capacity and uptakes significantly more lithium despite being the heaviest is highly intriguing. To address this question, we embark on investigating the thermodynamic stability in this family of compounds.

Thermodynamic Studies. Thermochemical data are sensitive to the crystal structure, phase, and chemical purity of the sample. PXRD and TG-DSC measurements were performed before the calorimetric measurement to detect any possible contamination/decomposition and check for adsorbed

water on the sample due to exposure in the ambient atmosphere prior to calorimetric experiments. Samples were phase pure as shown in Figure 1a−d, and TGA measurements detected no mass loss, confirming there was no adsorbed water on the samples.

The drop solution enthalpy (ΔH_{ds}) and formation enthalpy from oxides ($\Delta H^{\circ}_{f,ox}$) of $MLi_2Ti_6O_{14}$ (M = 2Na, Sr, Ba, and Pb) as a function of Li uptake per unit formula are shown in Table 2 and Figure 2a,b. The enthalpy of drop solution of

Table 2. Drop Solution Enthalpies (ΔH_{ds}) in $3Na_2O \cdot 4MoO_3$ at 800 °C and Formation Enthalpies ($\Delta H^{\circ}_{f,ox}$) at 25 °C of $MLi_2Ti_6O_{14}$ (M = 2Na, Sr, Ba, and Pb) Titanates

sample	ΔH_{ds} (kJ/mol)	$\Delta H^{\circ}_{f,ox}$ (kJ/mol)
$Na_2Li_2Ti_6O_{14}$	502.41 ± 0.35(8)	−333.32 ± 4.91
$BaLi_2Ti_6O_{14}$	506.75 ± 0.57(8)	−323.54 ± 3.44
$SrLi_2Ti_6O_{14}$	498.16 ± 0.68(8)	−260.65 ± 3.15
$PbLi_2Ti_6O_{14}$	508.46 ± 0.46(8)	−157.81 ± 2.54
Li_2O	−77.21 ± 2.44[23]	
Na_2O	−195.90 ± 4.23[27]	
TiO_2	73.70 ± 0.39(6)[28]	
SrO	−127.48 ± 1.84[a]	
BaO	−181.22 ± 2.32[a]	
PbO	−14.34 ± 0.38 (6)[a]	
CO_2	37.40	

[a]This work. The value is the mean of the number of experiments indicated in parentheses; two standard deviations are given as errors.

PbO, SrO, and BaO is obtained from the drop solution enthalpy of lead oxide and strontium and barium carbonate ($SrCO_3$ and $BaCO_3$) at 800 °C using the thermochemical cycle in Tables S5 and S6 (Supporting Information). The enthalpies of drop solution of Li_2O, Na_2O, and TiO_2 are taken from our previous measurements.[23,27,28] The formation enthalpy ($\Delta H^{\circ}_{f,ox}$) of $MLi_2Ti_6O_{14}$ (M = 2Na, Sr, Ba, and Pb) is calculated from the thermochemical cycles in Table 3.

The ΔH_{ds} for lithium titanates is endothermic ranging from 498.16 ± 0.68 to 508.46 ± 0.46 kJ/mol, and $\Delta H^{\circ}_{f,ox}$ is exothermic ranging from −333.32 ± 4.91 to −157.81 ± 2.54 kJ/mol, confirming that the these materials are thermodynamically stable. ΔH_{ds} does not follow any regular trend but $\Delta H^{\circ}_{f,ox}$ is inversely proportional to lithium uptake in $MLi_2Ti_6O_{14}$ (Figure 2b). The least stable $PbLi_2Ti_6O_{14}$ ($\Delta H^{\circ}_{f,ox}$ = −157.81 ± 2.54 kJ/mol) intercalates the most lithium (4.4 Li), followed by $Sr_2Li_2Ti_6O_{14}$ ($\Delta H^{\circ}_{f,ox}$ = −260.65 ± 3.15 kJ/mol, 3.08 Li), then $Ba_2Li_2Ti_6O_{14}$ ($\Delta H^{\circ}_{f,ox}$ = −323.54 ± 3.44 kJ/mol, 2.47 Li), while the most stable $Na_2Li_2Ti_6O_{14}$ ($\Delta H^{\circ}_{f,ox}$ = −333.32 ± 4.91 kJ/mol) inserts the least lithium (1.32 Li). Factors such as size of the metal ion, geometrical and compressive strains, and "acid−base" interaction explains their stability trend.

The energetics of ternary oxide formation is dominated by the difference in the acid−base character of the cations.[29] Binary oxides are classified as acidic, basic, or amphoteric. Smith's table[30] expresses all metal oxides in terms of acidity and the enthalpies of formation from binary oxides for lithium titanates change linearly with acidity. This validates the trends observed in the formation enthalpies, and in turn the lithium uptake (Figure 2c). The highly exothermic heats of formation reflect strong acid−base interactions among the MO, and Li_2O (basic oxides) with TiO_2 (a somewhat acidic oxide). The basic binary oxides MO and Li_2O interact with the acidic TiO_2 to form the $MLi_2Ti_6O_{14}$ structure. Alkali metal oxides exhibit greater basic character followed by alkaline earth metal oxides, among the divalent oxides those of larger cations are more basic compared to lighter cations, the order of basicity for MO is Na_2O > BaO > SrO.[31] Thus, the acid−base interaction between MO, Li_2O, and TiO_2 which stabilizes the structure most strongly in $Na_2Li_2Ti_6O_{14}$, followed by $BaLi_2Ti_6O_{14}$, then $SrLi_2Ti_6O_{14}$. This explains the trend observed in the $\Delta H^{\circ}_{f,ox}$ $Na_2Li_2Ti_6O_{14}$ > $BaLi_2Ti_6O_{14}$ > $SrLi_2Ti_6O_{14}$. This correlation is consistent with the dominance of the acid−base chemistry in phase stability, as seen in trends of enthalpies of formation in
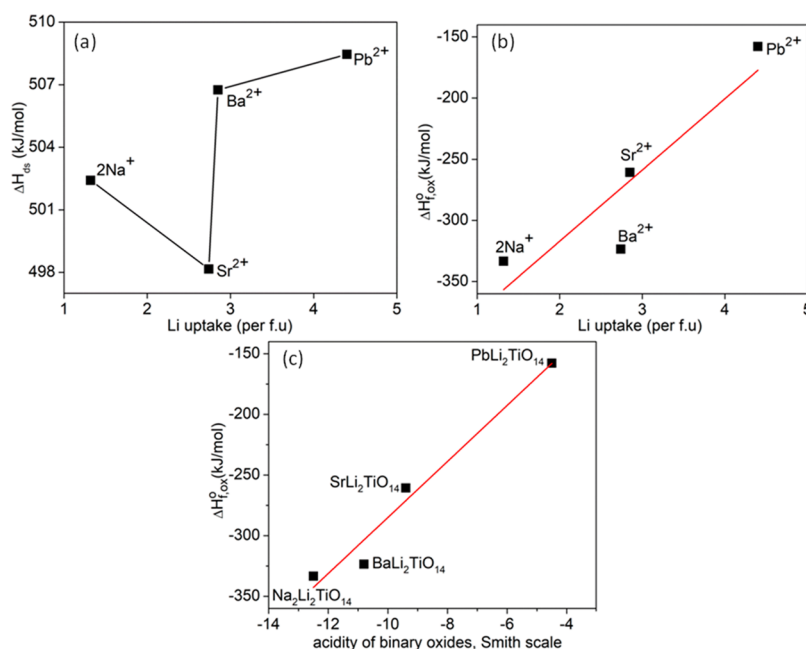

Figure 2. (a) Dissolution enthalpy (b) formation enthalpy vs reversible Li uptake (per formula unit) in the lithium titanates, and (c) enthalpies of formation from oxides for lithium titanates as a function of acidity based on Smith's scale of acidity for alkali, alkali-earth, and lead oxides.[30]

Table 3. Thermodynamic Cycles Used to Calculate Formation Enthalpies ($\Delta H^\circ_{f,ox}$) of $MLi_2Ti_6O_{14}$ at 25 °C

reaction	ΔH (kJ/mol)
$MLi_2Ti_6O_{14(S,25°C)} \rightarrow MO_{(soln,25°C)} + Li_2O_{(soln,25°C)} + 6TiO_{2(soln,25°C)}$	$\Delta H_1 = \Delta H_{ds}$ ($MLi_2Ti_6O_{14}$)
$Li_2O_{(S,25°C)} \rightarrow Li_2O_{(soln,25°C)}$	$\Delta H_2 = -77.21 \pm 2.44$[23]
$Na_2O_{(S,25°C)} \rightarrow Na_2O_{(soln,25°C)}$	$\Delta H_4 = -195.90 \pm 4.23$[27]
$TiO_{2(S,25°C)} \rightarrow TiO_{2(soln,25°C)}$	$\Delta H_3 = 73.70 \pm 0.39$[28]
$SrO_{(s,25°C)} \rightarrow SrO_{(soln,800°C)}$	$\Delta H_5 = -127.48 \pm 1.84$[a]
$BaO_{(s,25°C)} \rightarrow BaO_{(soln,800°C)}$	$\Delta H_6 = -181.22 \pm 2.32$[a]
$PbO_{(s,25°C)} \rightarrow PbO_{(soln,25°C)}$	$\Delta H_7 = -14.34 \pm 0.38$[a]
$MO_{(s,25°C)} + Li_2O_{(s,25°C)} + 6TiO_{2(s,25°C)} \rightarrow MLi_2Ti_6O_{14(s,25°C)}$	$\Delta H_8 = \Delta H^\circ_{f,ox}$ ($MLi_2Ti_6O_{14}$)
$\Delta H_8 = \Delta H^\circ_f(Na_2Li_2Ti_6O_{14}) = -\Delta H_1 + \Delta H_2 + 6\Delta H_3 + \Delta H_4$	
$\Delta H_8 = \Delta H^\circ_f(SrLi_2Ti_6O_{14}) = -\Delta H_1 + \Delta H_2 + 6\Delta H_3 + \Delta H_5$	
$\Delta H_8 = \Delta H^\circ_f(BaLi_2Ti_6O_{14}) = -\Delta H_1 + \Delta H_2 + 6\Delta H_3 + \Delta H_6$	
$\Delta H_8 = \Delta H^\circ_f(PbLi_2Ti_6O_{14}) = -\Delta H_1 + \Delta H_2 + 6\Delta H_3 + \Delta H_7$	

[a]This work.

many other compounds, including perovskites, olivines, tungstates, carbonates, nitrides and oxynitrides, and glasses.[29,30,32–36]

The enthalpy of formation from oxides is additionally influenced by the space constraints. In $Na_2Li_2Ti_6O_{14}$, monovalent sodium occupies the 11-fold site completely as opposed to the divalent counterparts which occupy only half of it. Thus, for the sodium compound, there is no vacant site available for further lithium insertion in the structure. However, in $MLi_2Ti_6O_{14}$ (M = Sr, Ba, and Pb), despite having similar, additional vacant sites, the divalent members uptake lithium differently. This could be due to size of the metal ions, acid–base interactions as discussed earlier, and the compressive strain induced by the ion at the 11-fold coordinated site. Low bond valence sum (BVS) for Sr (1.75) and Pb (1.79) indicates no residual strain at these sites whereas in Ba (2.11) due to its high BVS has a shortened Ba–O length which results in a compressive strain, strangulating the lithium pathway to interstitial sites.

The difference in the Li uptake by $MLi_2Ti_6O_{14}$ (M = Sr and Pb), regardless of having no compressive strain and similar ionic radii of Sr and Pb, is puzzling. The trend of decreasing stability in the $\Delta H^\circ_{f,ox}$ is $Na_2Li_2Ti_6O_{14}$ > $BaLi_2Ti_6O_{14}$ > $SrLi_2Ti_6O_{14}$ > $PbLi_2Ti_6O_{14}$. The low stability of $PbLi_2Ti_6O_{14}$ is attributed to the amphoteric nature of PbO. Consequently, the acid–base interaction between PbO, Li_2O, and TiO_2 is weak compared to alkali and alkaline earth metal oxides; thus, there is decline in the stability of $PbLi_2Ti_6O_{14}$. Similar differences are seen in comparing lead and strontium silicate glasses.[37] This is in corroboration to the Smith's scale of acidity.

Depending on the stability of these lithium titanates, the amount of Li uptake varies during charge cycles. The least stable $PbLi_2Ti_6O_{14}$ gains stability by intercalating 4.4 Li, whereas the slightly more stable $SrLi_2Ti_6O_{14}$ intercalates only 2.9 Li. The most stable $SrLi_2Ti_6O_{14}$ and $Na_2Li_2Ti_6O_{14}$ intercalate 2.7 and 1.3 Li. Future calorimetric measurements on samples with intermediate charge cycles having a variable amount of Li in the 11-coordination site for the $MLi_2Ti_6O_{14}$ (M = Ba, Sr, and Pb) structures would provide more insight into the stability.

CONCLUSIONS

It can be concluded that there is strong correlation between the thermodynamic stability and the lithium uptake in this class of materials. Strong exothermic acid–base reactions between MO, Li_2O, and TiO_2 result in large exothermic

enthalpies of formation, indicating that $MLi_2Ti_6O_{14}$ are thermodynamically stable. Depending on the nature of acid–base interactions, the stability varies, alkali metals exhibit greater basic character followed by alkaline earth metal oxides, and among the alkaline earth metal oxides, those of larger cations are more basic compared to lighter cations, and the order of basicity for MO is Na_2O > BaO > SrO. PbO is an amphoteric oxide for which the acid–base interaction is weak compared to alkali or alkaline earth metal oxides. Thus, the thermodynamic stability diminishes in the order $Na_2Li_2Ti_6O_{14}$ > $BaLi_2Ti_6O_{14}$ > $SrLi_2Ti_6O_{14}$ > $PbLi_2Ti_6O_{14}$ which is directly proportional to the acid–base interactions. The trends in stability also depend on the charge and size of the cation and the compressive strain which are typical for interoxidic compounds. The formation enthalpy in these materials is inversely proportional to the lithium uptake during charge cycles. Least stable $PbLi_2Ti_6O_{14}$ uptakes most Li (4.4 Li), and the most stable $Na_2Li_2Ti_6O_{14}$ uptakes least Li (1.3 Li).

ASSOCIATED CONTENT

Ⓢ Supporting Information

The Supporting Information is available free of charge at https://pubs.acs.org/doi/10.1021/acsomega.2c05701.

> Rietveld refinement of $MLi_2Ti_6O_{14}$ (M = Sr, Ba, and 2Na) titanates and thermodynamic cycles used to calculate the drop solution enthalpy (ΔH_{ds}) of SrO and BaO in sodium molybdate at 800 °C (PDF)

AUTHOR INFORMATION

Corresponding Author

Alexandra Navrotsky − *School of Molecular Sciences and Navrotsky Eyring Center for Materials of the Universe, Arizona State University, Tempe, Arizona 85287, United States;* ⓘ orcid.org/0000-0002-3260-0364; Email: Alexandra.Navrotsky@asu.edu

Authors

K. Jayanthi − *School of Molecular Sciences and Navrotsky Eyring Center for Materials of the Universe, Arizona State University, Tempe, Arizona 85287, United States; Chemical Sciences Division, Oak Ridge National Laboratory, Oak Ridge, Tennessee 37831, United States;* ⓘ orcid.org/0000-0002-5016-3575

Anshuman Chaupatnaik − *Faraday Materials Laboratory, Materials Research Centre, Indian Institute of Science,*

Bangalore 560012, India; Chimie du Solide-Energie, UMR 8260, Collège de France, Paris 75001, France

Prabeer Barpanda − *Faraday Materials Laboratory, Materials Research Centre, Indian Institute of Science, Bangalore 560012, India; Helmholtz Institute Ulm (HIU), Electrochemical Energy Storage, Ulm 89081, Germany; Institute of Nanotechnology, Karlsruhe Institute of Technology (KIT), Karlsruhe 76021, Germany;* ⊙ orcid.org/0000-0003-0902-3690

Complete contact information is available at:
https://pubs.acs.org/10.1021/acsomega.2c05701

Notes

The authors declare no competing financial interest.

■ REFERENCES

(1) Goodenough, J. B.; Park, K. S. The Li-ion rechargeable battery: A perspective. *J. Am. Chem. Soc.* **2013**, *135*, 1167−1176.

(2) Whittingham, M. S. Electrical energy storage and intercalation chemistry. *Science* **1976**, *192*, 1126−1127.

(3) Ohzuku, T.; Iwakoshi, Y.; Sawai, K. Formation of lithium-graphite intercalation compounds in nonaqueous electrolytes and their application as a negative electrode for a lithium ion (shuttlecock) cell. *J. Electrochem. Soc.* **1993**, *140*, 2490−2498.

(4) Aurbach, D.; Cohen, Y.; Teller, H. A short review of failure mechanisms of lithium metal and lithiated graphite anodes in liquid electrolyte solutions. *Solid State Ionics* **2002**, *148*, 405−416.

(5) Winter, M.; Barnett, B.; Xu, K. Before Li ion batteries. *Chem. Rev.* **2018**, *118*, 11433−11456.

(6) Fong, R.; Sacken, U.; Dahn, J. R. Studies of lithium intercalation into carbons using nonaqueous electrochemical cells. *J. Electrochem. Soc.* **1990**, *137*, 2009−2013.

(7) Han, J. T.; Huang, Y. H.; Goodenough, J. B. New anode framework for rechargeable batteries. *Chem. Mater.* **2011**, *23*, 2027−2029.

(8) Colbow, K. M.; Dahn, J. R.; Haering, R. R. Structure and electrochemistry of the spinel oxides $LiTi_2O_4$ and $Li_{4/3}Ti_{5/3}O_4$. *J. Power Sources* **1989**, *26*, 397−402.

(9) Ohzuku, T.; Ueda, A.; Yamamoto, N. Zero-strain insertion material of $Li[Li_{1/3}Ti_{5/3}]O_4$ for rechargeable lithium cells. *J. Electrochem. Soc.* **1995**, *142*, 1431−1435.

(10) Zaghib, K.; Dontigny, M.; Guerfi, A.; Charest, P.; Rodrigues, I.; Mauger, A.; Julien, C. M. Safe and fast-charging Li-ion battery with long shelf life for power applications. *J. Power Sources* **2011**, *196*, 3949−3954.

(11) Liu, S.; Yan, L.; Lan, H.; Yu, H.; Qian, D.; Cheng, X.; Long, N.; Shui, M.; Shu, J. Investigation of $Li_5Cr_7Ti_6O_{25}$ as novel anode material for high-power lithium-ion batteries. *Ceram. Int.* **2017**, *43*, 7908−7915.

(12) Patoux, S.; Masquelier, C. Lithium insertion into titanium phosphates, silicates, and sulfates. *Chem. Mater.* **2002**, *14*, 5057−5068.

(13) Zhu, G.; Wang, Y.; Xia, Y. Ti-based compounds as anode materials for Li-ion batteries. *Energy Environ. Sci.* **2012**, *5*, 6652−6667.

(14) Chen, Z.; Belharouak, I.; Sun, Y.-K.; Amine, K. Titanium-based anode materials for safe lithium-ion batteries. *Adv. Funct. Mater.* **2013**, *23*, 959−969.

(15) Belharouak, I.; Amine, K. $Li_2MTi_6O_{14}$ (M = Sr, Ba): New anodes for lithium-ion batteries. *Electrochem. Commun.* **2003**, *5*, 435−438.

(16) Dambournet, D.; Belharouak, I.; Amine, K. $MLi_2Ti_6O_{14}$ (M = Sr, Ba, 2Na) lithium insertion titanate materials: A comparative study. *Inorg. Chem.* **2010**, *49*, 2822−2826.

(17) Li, P.; Qian, S.; Yu, H.; Yan, L.; Lin, X.; Yang, K.; Long, N.; Shui, M.; Shu, J. $PbLi_2Ti_6O_{14}$: A novel high-rate long-life anode material for rechargeable lithium-ion batteries. *J. Power Sources* **2016**, *330*, 45−54.

(18) Dambournet, D.; Belharouak, I.; Ma, J.; Amine, K. Template-assisted synthesis of high packing density $SrLi_2Ti_6O_{14}$ for use as anode in 2.7-V lithium-ion battery. *J. Power Sources* **2011**, *196*, 2871−2874.

(19) Yi, T.-F.; Zhu, Y.-R.; Tao, W.; Luo, S.; Xie, Y.; Li, X.-F. Recent advances in the research of $MLi_2Ti_6O_{14}$ (M = 2Na, Sr, Ba, Pb) anode materials for Li-ion batteries. *J. Power Sources* **2018**, *399*, 26−41.

(20) Navrotsky, A. Progress and new directions in high temperature calorimetry. *Phys. Chem. Miner.* **1997**, *2*, 89−104.

(21) Navrotsky, A. Progress and new directions in high temperature calorimetry revisited. *Phys. Chem. Miner.* **1997**, *24*, 222−241.

(22) Navrotsky, A. Progress and new Directions in calorimetry: A 2014 perspective. *J. Am. Ceram. Soc.* **2014**, *97*, 3349−3359.

(23) Abramchuk, M.; Voskanyan, A. A.; Arinicheva, Y.; Lilova, K.; Subramani, T.; Ma, Q.; Dashjav, E.; Finsterbusch, M.; Navrotsky, A. Energetic stability and its role in the mechanism of ionic transport in NASICON-type solid-state electrolyte $Li_{1+x}Al_xTi_{2−x}(PO_4)_3$. *J. Phys. Chem. Lett.* **2021**, *12*, 4400−4406.

(24) Chung, S. L.; Wang, C. M. Solution combustion synthesis of TiO_2 and its use for fabrication of photoelectrode for dye-sensitized solar cell. *J. Mater. Sci. Technol.* **2012**, *28*, 713−722.

(25) Von Dreele, R. B.; Larson, A. C. General structure analysis system (GSAS). *Los Alamos Natl. Lab. Rep. LAUR* **2004**, *748*, 86−748.

(26) Momma, K.; Izumi, F. VESTA: a three-dimensional visualization system for electronic and structural analysis. *J. Appl. Crystallogr.* **2008**, *41*, 653−658.

(27) Yang, S.; Andreko, A.; Riman, R.; Navrotsky, A. Thermochemistry of sodium rare earth ternary fluorides, $NaREF_4$. *Acta Mater.* **2021**, *220*, No. 117289.

(28) Hayun, S.; Tran, T. B.; Lian, J.; Fuentes, A. F.; Navrotsky, A. Energetics of stepwise disordering transformation in pyrochlores, $RE_2Ti_2O_7$ (RE = Y, Gd and Dy). *Acta Mater.* **2012**, *60*, 4303−4310.

(29) Navrotsky, A. Repeating patterns in mineral energetic. *Am. Mineral.* **1994**, *79*, 589−605.

(30) Smith, D. W. An acidity scale for binary oxides. *J. Chem. Educ.* **1978**, *64*, 480−481.

(31) David Jackson, S.; Hargreaves, J. S. J. *Metal Oxide Catalysis*; Wiley: Germany, 2008; Vol. *1*, ch. 3, pp 167−168.

(32) Sahu, S. K.; Zlotnik, S.; Navrotsky, A.; Vilarinho, P. M. Thermodynamic stability of lead-free alkali niobate and tantalite Perovskites. *J. Mater. Chem. C* **2015**, *3*, 7691−7698.

(33) Nhu, S.; Navrotsky, A. Energetics of formation of alkali and ammonium cobalt and zinc phosphate frameworks. *J. Solid State Chem.* **2008**, *181*, 20−29.

(34) Navrotsky, A. Thermochemical studies of nitrides and oxynitrides by oxidative oxide melt calorimetry. *J. Alloys Compd.* **2001**, *321*, 300−306.

(35) Shvareva, T. Y.; Fein, J. B.; Navrotsky, A. Thermodynamic properties of uranyl minerals: constraints from calorimetry and solubility measurements. *Ind. Eng. Chem. Res.* **2012**, *5*, 607−613.

(36) Wu, L.; Koryttseva, A.; Groß, C. B. M.; Navrotsky, A. Thermochemical investigation of lithium borate glasses and crystals. *J. Am. Ceram. Soc.* **2019**, *102*, 4538−4545.

(37) Roy, B. N.; Navrotsky, A. Thermochemistry of charge-coupled substitutions in silicate glasses: The systems $M_{l/n}{}^{n+}AlO_2{}^{-}SiO_z$ (M = Li, Na, K, Rb, Cs, Mg, Ca, Sr, Ba, Pb). *J. Am. Ceram. Soc.* **1984**, *67*, 606−610.